Supplementary Information

Hybrid nanoparticles as theranostics platforms for glioblastoma treatment: phototherapeutic and X-ray phase contrast tomography investigations

Loredana Ricciardi [1,*], Sharmistha Chatterjee [2], Giovanna Palermo [2,1], Elisabeta I. Szerb [3], Alessia Sanna [4], Francesca Palermo [4,2], Nicola Pieroni [4], Michela Fratini [4], Roberto Bartolino [1], Alessia Cedola [4], Massimo La Deda [5,1,6,*] and Giuseppe Strangi [7,1,2,*]

[1] CNR NANOTEC- Institute of Nanotechnology U.O.S. Cosenza, 87036 Rende, CS, Italy;
[2] Department of Physics, University of Calabria, 87036 Rende, CS, Italy;
[3] "Coriolan Dragulescu" Institute of Chemistry, Romanian Academy, 24 Mihai Viteazu Bvd., 300223 Timisoara, Romania;
[4] CNR NANOTEC- Institute of Nanotechnology U.O.S. Roma, Piazzale Aldo Moro 5, 00185 Roma, Italy;
[5] Department of Chemistry and Chemical Technologies, University of Calabria, 87036 Rende, CS, Italy;
[6] National Interuniversity Consortium of Materials Science and Technology, LASCAMM, Calabria Unit, 87036 Rende, CS, Italy;
[7] Department of Physics and Case Comprehensive Cancer Center, Case Western Reserve University, 10600 Euclid Avenue, Cleveland, Ohio 44106, USA
* Correspondence: loredana.ricciardi@cnr.it (L.R.); massimo.ladeda@unical.it (M.L.D.); giuseppe.strangi@case.edu (G.S.)

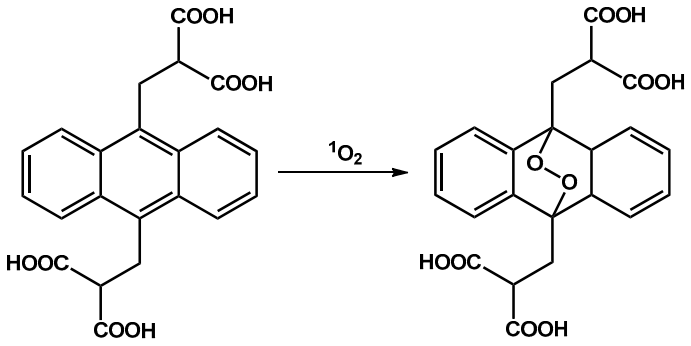

Scheme S1. Chemical reaction of ABDA with singlet oxygen.

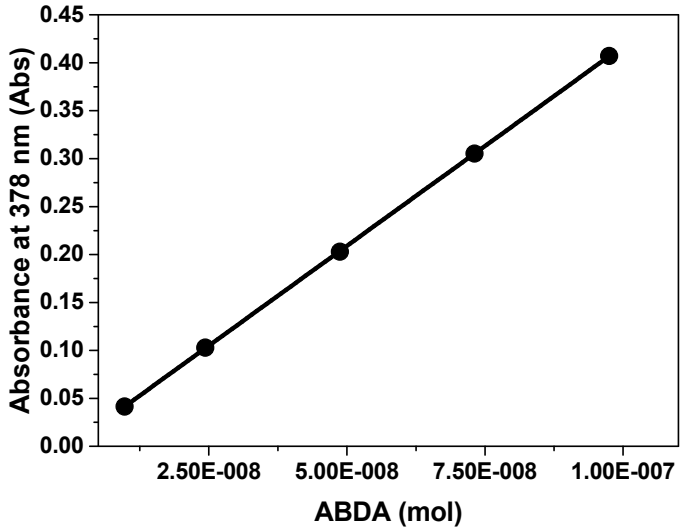

Figure S1. Correlation between optical density and molar concentration of ABDA. Absorbance as a function of number of moles of ABDA present in solution.

(**a**) (**b**)

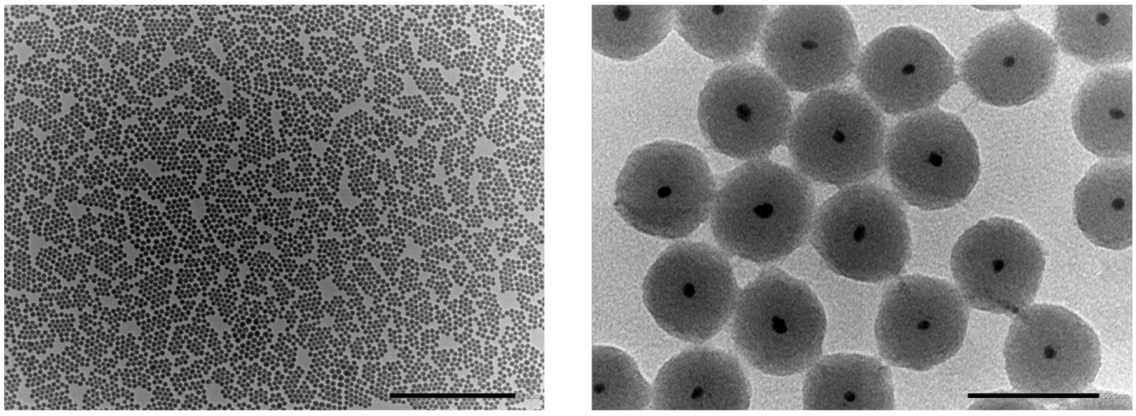

Figure S2. Morphological characterization of the photo-therapeutic nanoplatform. (**a**) TEM image (scale bar, 1 μm) and (**b**) higher magnification of **Ir$_1$-AuSiO$_2$** (scale bar, 50 nm).

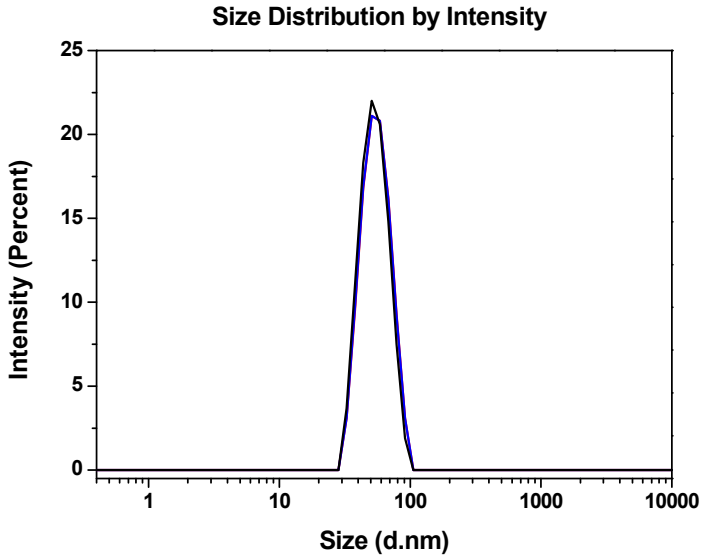

Figure S3. Nanoparticles analysis via Dynamic Light Scattering. Hydrodynamic size and size distribution of **Ir$_1$-AuSiO$_2$**.

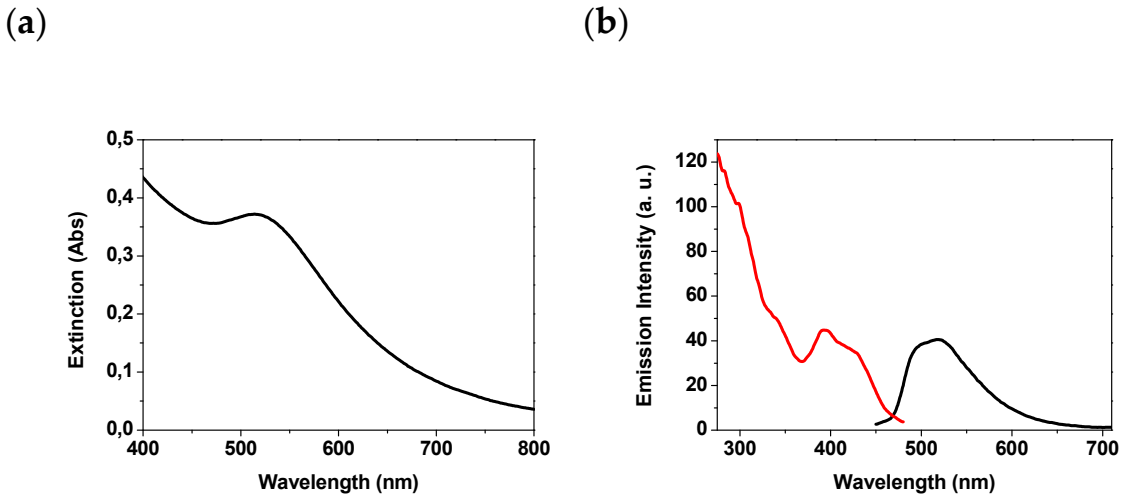

Figure S4. Photophysical characterization of **Ir$_1$-AuSiO$_2$**. (**a**) Extinction (**b**) excitation and emission spectra of **Ir$_1$-AuSiO$_2$** in aqueous solution at room temperature (λ_{ex}= 420 nm; λ_{em}= 520 nm).

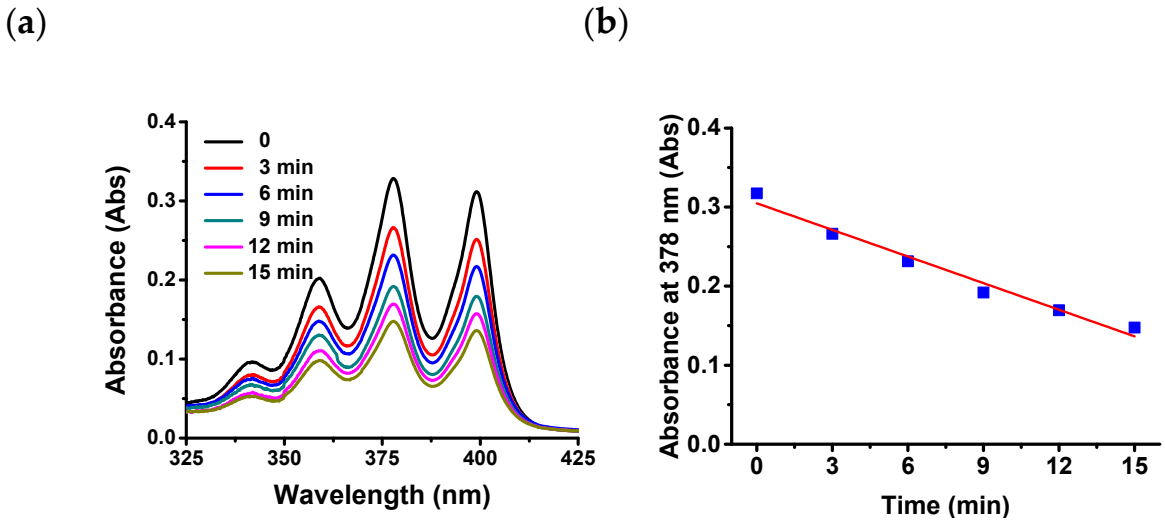

Figure S5. Detection of $^1O_2$ generation of Pc4 by ABDA method. (**a**) Photobleaching of ABDA by $^1O_2$ at different irradiation times (0 - 15 min) in water, and in presence of Pc4 ([Pc4]=2 × 10^{-5} M). The experiments were carried out by using an excitation source at 365 nm - 20 mW; (**b**) plotting of ABDA absorption at 378 nm as a function of the illumination time.

Ir_1: preimage

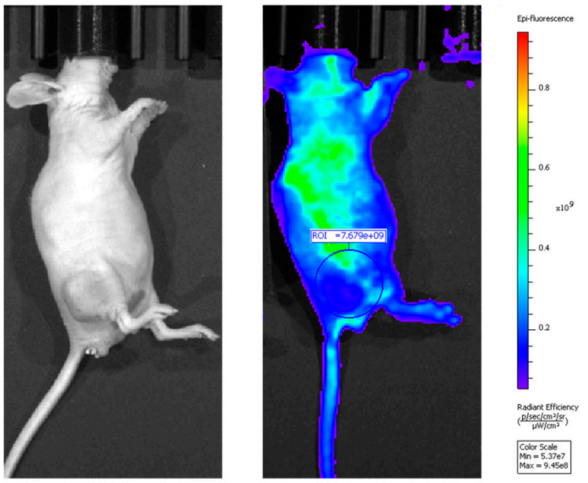

Ir_1: 15 min

Ir_1: 30 min

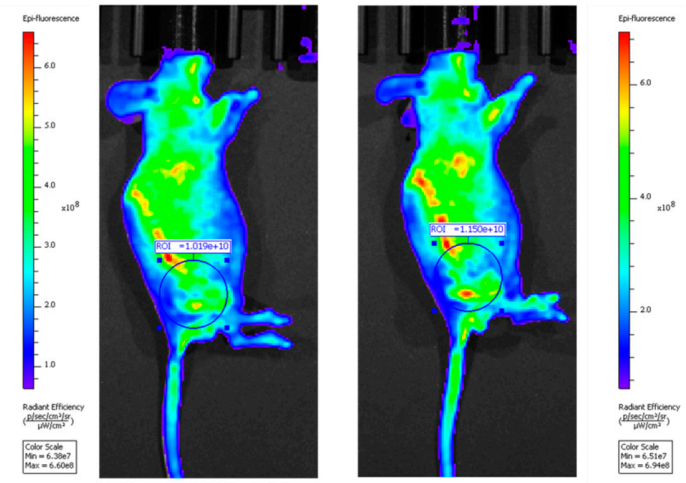

Ir_1: 90 min

Ir_1: 24 h

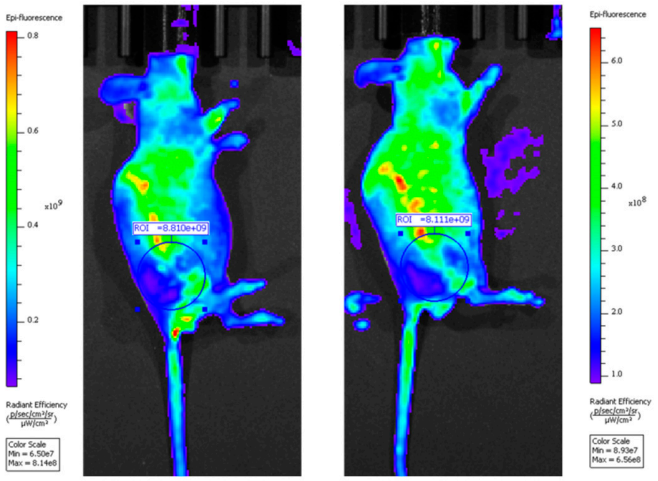

Figure S6. Post-injection trafficking of **Ir1** analyzed via *in vivo* imaging. Fluorescence scans of mice intratumorally injected with 200 μL of **Ir1** ([Ir1]= 2×10^{-5} M), acquired before administration (preimage), and at different time points post-injection (15, 30, 90 min and 24 h).

Ir_1-$AuSiO_2$: preimage

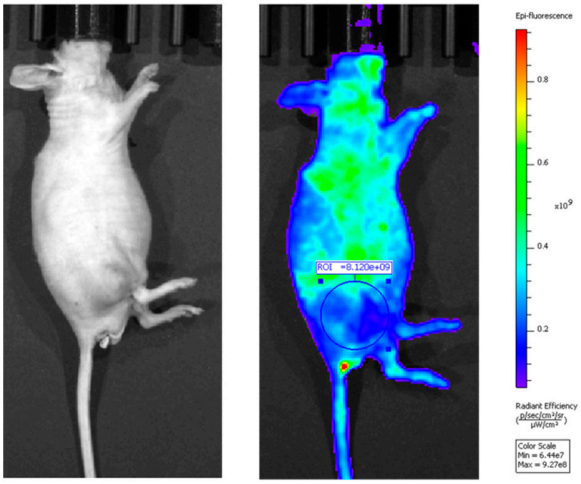

Ir_1-$AuSiO_2$: 15 min

Ir_1-$AuSiO_2$: 30 min

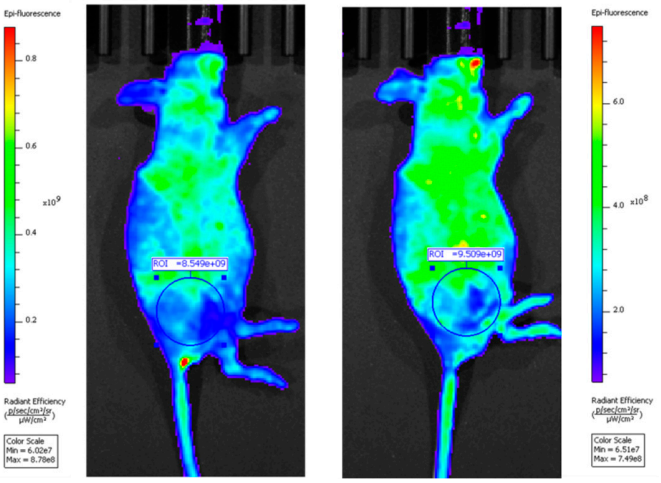

Ir_1-$AuSiO_2$: 90 min

Ir_1-$AuSiO_2$: 24 h

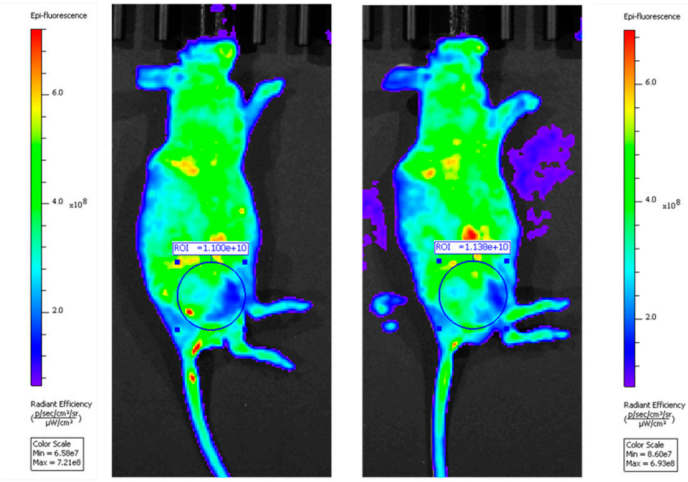

Figure S7. Post-injection trafficking of **Ir_1-AuSiO$_2$** analyzed via *in vivo* imaging. Fluorescence scans of mice intratumorally injected with 200 μL of **Ir_1-AuSiO$_2$** ([Ir_1]= 2×10^{-5} M), acquired before administration (preimage), and at different time points post-injection (15, 30, 90 min and 24 h).

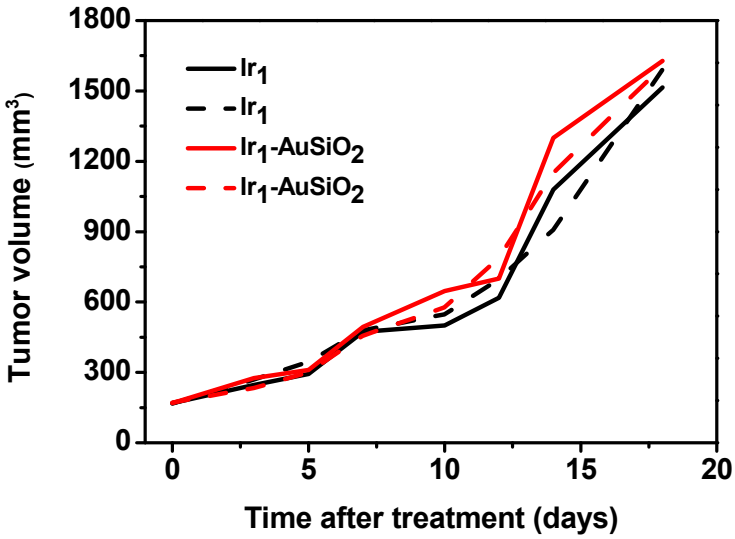

Figure S8. Control groups - Follow-up of GBM xenograft mice treated with **Ir_1** or **Ir_1-AuSiO$_2$** in absence of optical radiation dose. Time-dependent tumor growth curves after intratumoral injection of **Ir_1** or **Ir_1-AuSiO$_2$** in GBM-bearing mice (n= 2 mice per group) kept in the darkness and in absence of any light exposure. Solid or dotted lines were used to better distinguish the tumor growth curves of mice within each group.

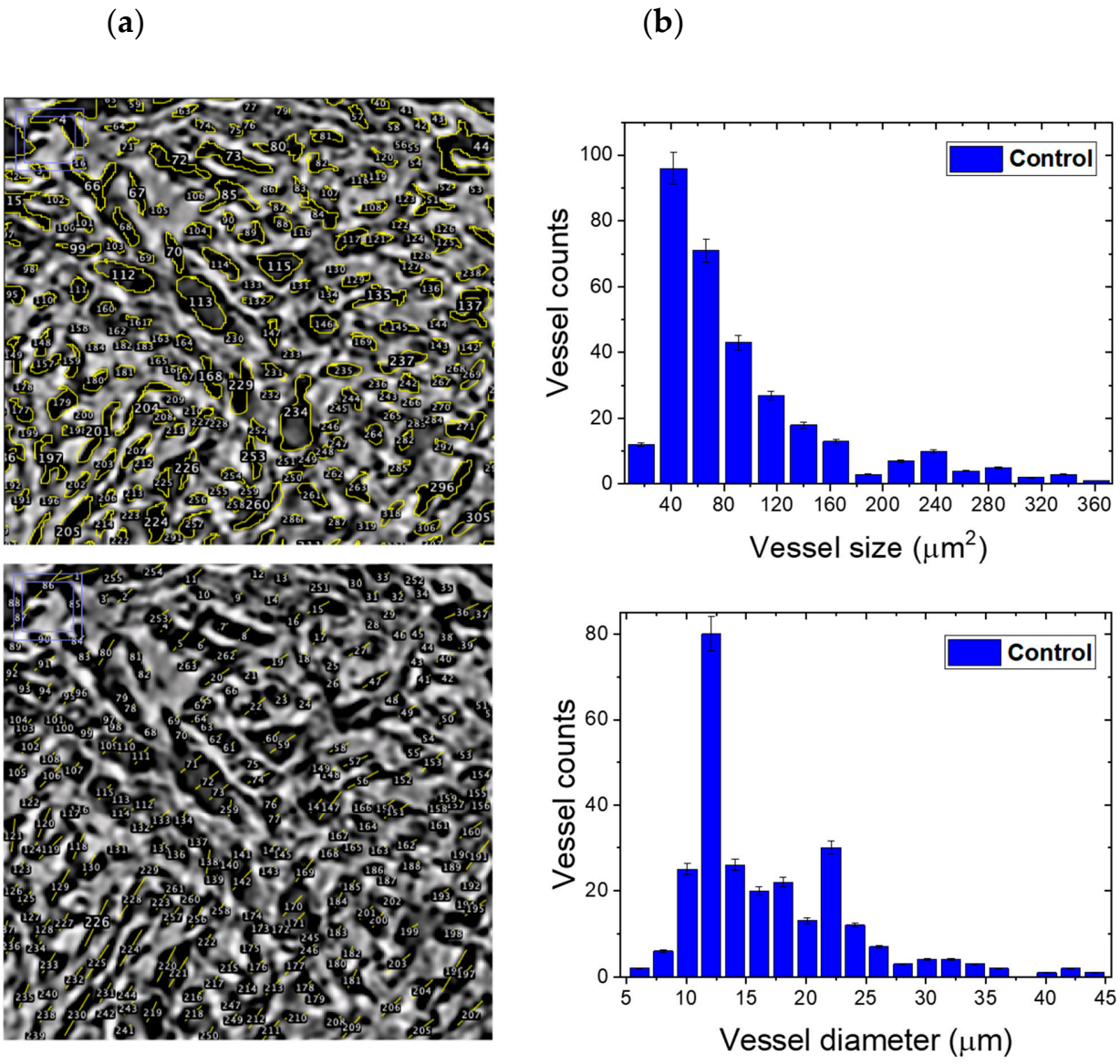

Figure S9. X-ray phase contrast tomography images and quantitative analysis of the vascular network of *ex vivo* GBM sample treated only with the radiation dose. (**a**) Tomography images (400 × 400 pixels) of a GBM slice (control) and (**b**) related quantitative measurements. Image and graph in the top are referred to the vessel size, while image and graph in the bottom are referred to the vessel diameter.

(**a**) (**b**)

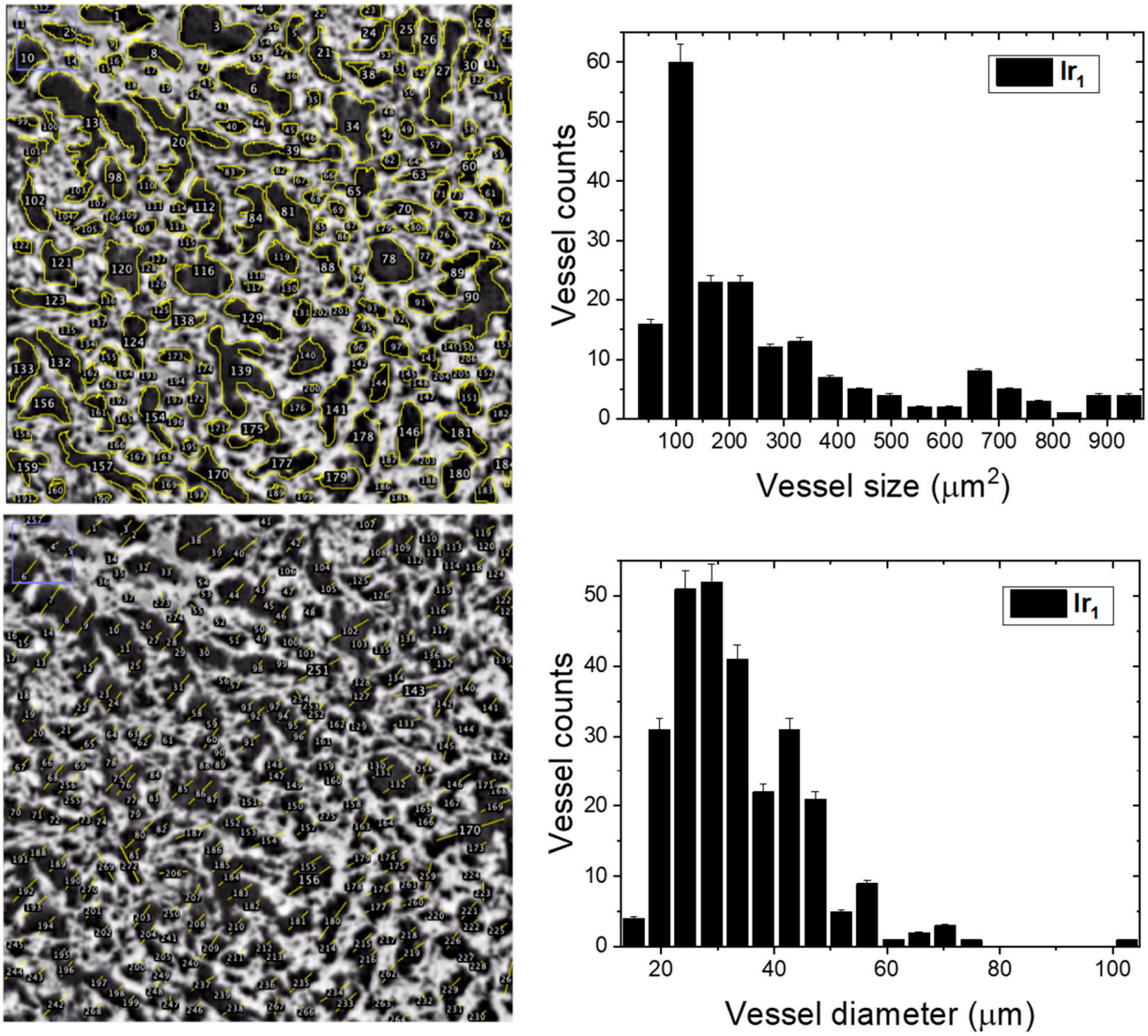

Figure S10. X-ray phase contrast tomography images and quantitative analysis of the vascular network of *ex vivo* GBM sample treated with **Ir**$_1$ + light exposure. (**a**) Tomography images (400 × 400 pixels) of a GBM slice treated with **Ir**$_1$ + light exposure and (**b**) related quantitative measurements. Image and graph in the top are referred to the vessel size, while image and graph in the bottom are referred to the vessel diameter.

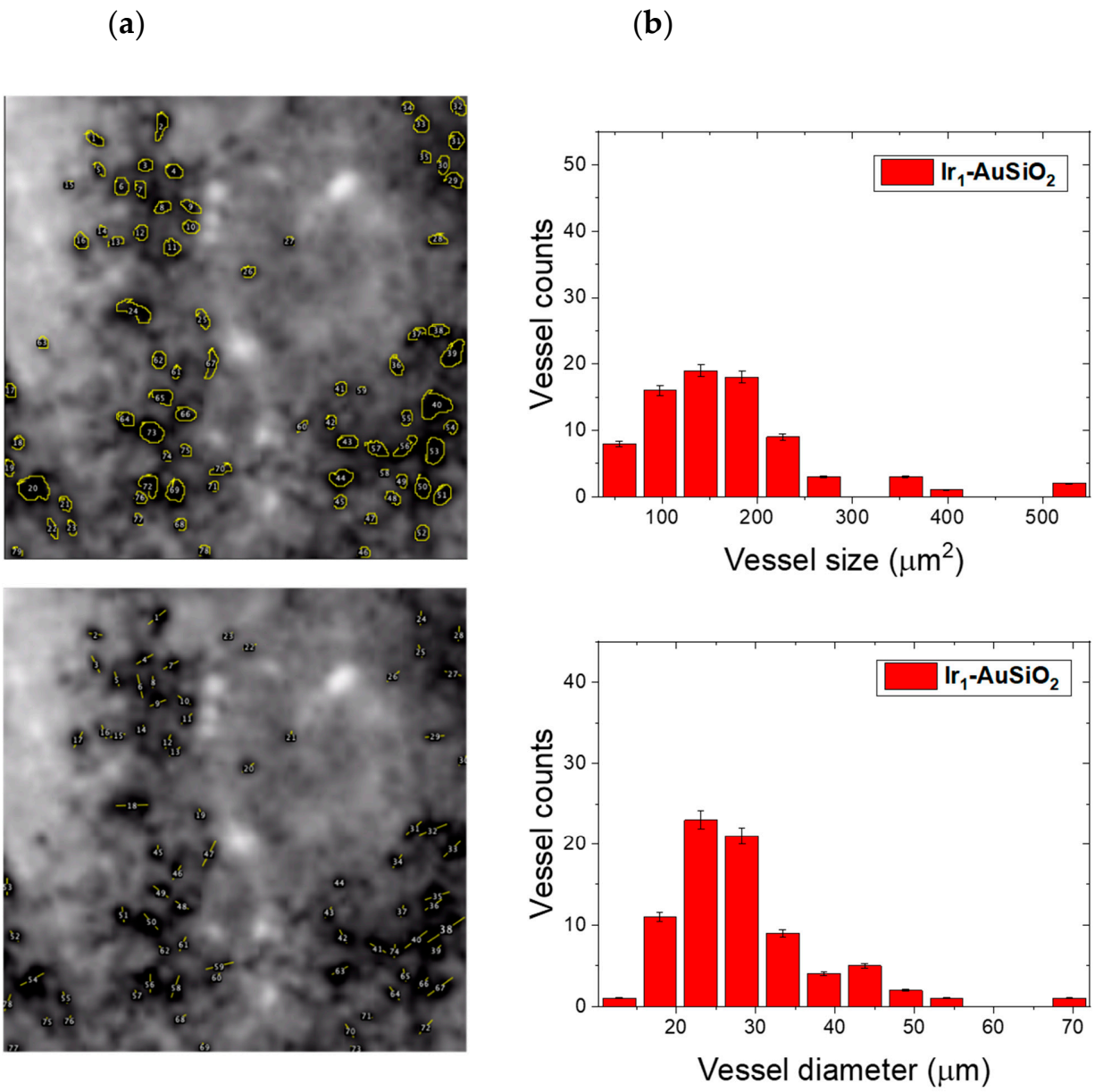

Figure S11. X-ray phase contrast tomography images and quantitative analysis of the vascular network of *ex vivo* GBM sample treated with **Ir$_1$-AuSiO$_2$** + light exposure. (**a**) Tomography images (400 × 400 pixels) of a GBM slice treated with **Ir$_1$-AuSiO$_2$** + light exposure and (**b**) related quantitative measurements. Image and graph in the top are referred to the vessel size, while image and graph in the bottom are referred to the vessel diameter.

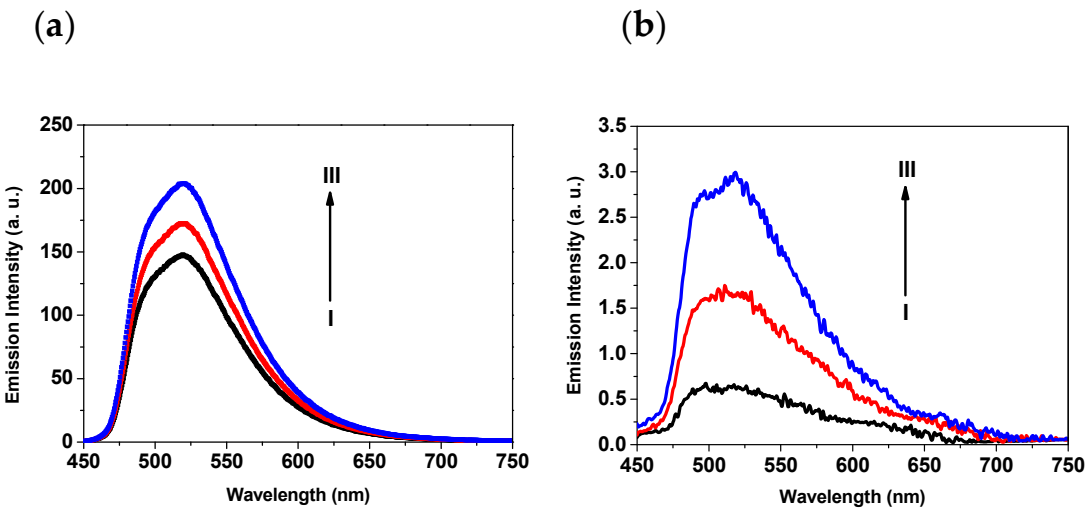

Figure S12. Emission spectra of (**a**) **Ir**$_1$ and (**b**) **Ir**$_1$**-AuSiO**$_2$ in water solution at different concentrations of Ir$_1$: 2 × 10^{-5} M (I); 1.33 × 10^{-5} M (II); 8.8 × 10^{-6} M (III), λ_{ex}= 430 nm.

Video S1. Three-dimensional volume (350 × 350 × 350 μm^3) of GBM sample after intratumoral injection of **Ir**$_1$**-AuSiO**$_2$ followed by light exposure. The microvasculature is rendered in red and the **Ir**$_1$**-AuSiO**$_2$ clusters in yellow.